Time-resolved thermal transport in compositionally modulated metal films

Bruce M. Clemens, Gary L. Eesley, and Carolyn A. Paddock*
Physics Department, General Motors Research Laboratories, Warren, Michigan 48090-9055
(Received 27 July 1987)

We report on investigations of one-dimensional thermal transport in compositionally modulated metal films produced with a systematic variation in atomic lattice mismatch. In the case of Ni-Cu, Ni-Mo, Ni-Ti, and Ni-Zr, we observe the relative effects of interfacial disorder on thermal diffusion. Our observations demonstrate the thermal impedance of a single metal-metal interface and indicate that thermal diffusion in a bilayer film is strongly influenced by the interface between contacting metal pairs. This study is made possible by picosecond time-resolved thermoreflectance measurements which probe thermal transport perpendicular to the film plane. This technique can impact on our understanding of electron scattering and transport across metallic boundaries, and it provides a means of inferring electrical transport properties.

I. INTRODUCTION

New material growth processes such as molecular-beam epitaxy and ion sputter deposition have resulted in the production of material structures with compositional modulations on the atomic scale. The intense effort to characterize these materials is driven in anticipation of new and potentially useful elastic, electrical, and thermal properties. In the case of compositionally modulated semiconductors, the modification of the electrical and optical properties is well documented.[1] However, the study of modulated metal films has only recently gained widespread attention.[2–4]

It is known that in metallic multilayer films, the electrical transport properties are perturbed by electron scattering off of the altered periodic potential of an interface. The deviation in crystal structure parallel and perpendicular to an interface results from different binding forces on either side of the interface. As a result, the details of the electron scattering are influenced by both the interfacial structure and the direction of transport.[5–10] Unfortunately, electrical transport perpendicular to a thin-film plane is difficult to measure directly. It is usually inferred from conventional four-point probe techniques which measure the effective transport parallel to the film plane.[7,10]

Previously we reported on a transient thermoreflectance (TTR) technique which is capable of measuring thermal diffusion in metal films.[11] The measurement is optical and noncontacting, and does not require thermal isolation of the substrate from the supported film. An important feature of our technique is the ability to measure transport perpendicular to the film plane, with sufficient sensitivity to probe the thermal impedance of a metallic interface. As a result, such studies can impact on our understanding of electron scattering and transport across metallic boundaries. In the event that transport in multilayer structures obeys the Weidemann-Franz relationship, then the electrical transport properties can be inferred from thermal transport measurements.[12]

Our purpose in this study is to investigate the effect of interfacial structure on thermal transport. This study is motivated by measurements of thermal transport in multilayer metal films which exhibit a substantial decrease in thermal diffusivity relative to that measured in the constituent single-element films.[11] These observations suggest that the interface between two different metals can alter thermal transport in a manner analogous to that observed in the case of electrical transport.[7] This is not so surprising in light of the intimate relationship between the electrical and thermal conductivities of a metal.

In this paper we use TTR to study the thermal transport properties of the metal pairs Ni-Cu, Ni-Mo, Ni-Ti, and Ni-Zr. These pairs were chosen to produce a systematic variation in lattice mismatch and interfacial disorder. Both multilayer and bilayer samples were fabricated, and the sample structure was investigated by x-ray diffraction measurements. By measuring the thermal transport in the bilayer and single-element reference films, we demonstrate the impedance of thermal transport by a single metal-metal interface. We have developed a numerical model for thermal transport in the bilayer films, and we present semiquantitative results for the impedance of a Ni-Ti and a Ni-Zr interface.

II. TECHNIQUE AND MODEL

Our measurement of thermal transport in metal films is based upon the thermally-induced change in optical reflectivity (thermoreflectance).[13] We generate a thermoreflectance signal by means of two synchronous laser pulses which are used to heat the sample surface and to measure the resulting change in reflectivity. By using picosecond duration laser pulses, we can rapidly heat a metal and perform a time-resolved measurement of thermal diffusion by sequentially delaying the probing pulse relative to the heating pulse. Since the energy from the heating pulse is absorbed in a volume roughly 20 μm in diameter and 15 nm in depth, the thermal gradient perpendicular to the film plane will dominate the

 ©1988 The American Physical Society

thermal transport. Diffusion out of this region requires a few hundred picoseconds, and for film thicknesses on the order of 100 nm or larger the TTR measurement is completed before substrate effects become important.

The thermally-induced change in reflectivity is described by the temperature derivative of the Fresnel reflection formula

$$\frac{dR}{dT}=\frac{4[2nk(dk/dT)-(1-n^2+k^2)(dn/dT)]}{[(1+n)^2+k^2]^2}, \quad (1)$$

where R is the normal incidence reflectivity, T is the temperature, and n and k are the real and imaginary parts of the metal refractive index, respectively. The reflectivity change is linearly proportional to the temperature derivative of the refractive index, and for small temperature excursions this derivative is constant.[14] As a general rule, the reflectivity of a metal will decrease with increasing temperature. This situation is analogous to the decrease in electrical conductivity with increasing temperature, and it is the result of an increased electron-phonon collision frequency.[12] Exceptions can occur in the optical regime when photon energies coincide with interband transition energies.[13]

As a result of the linear relationship in Eq. (1), the temporal response of the thermoreflectance signal is directly related to the surface temperature. Thus to the extent that thermal barriers within the film perturb the time evolution of the temperature gradient near the surface, a thermoreflectance measurement will be sensitive to the presence of such barriers. Several heat flow models have been proposed which include both an intrinsic and extrinsic thermal impedance to transport across boundaries where there is an abrupt change in thermal properties.[15–17] In a similar manner, we have modified our thermal transport model to include interfacial impedance, while retaining the essential features of our measurement scheme (volume heating and finite pulse width).[11] The resulting one-dimensional model can be used to analyze our TTR measurements of thermal diffusion in the bilayer films.

The transport of heat through a bilayer can be described by two heat-conduction equations which are valid within each single-element layer. In the top layer, the temperature as a function of time and depth is given by

$$c_1\frac{\partial\Delta T_1(z,t)}{\partial t}=K_1\frac{\partial^2\Delta T_1(z,t)}{\partial z^2}+I(1-R_1)\alpha_1 e^{-\alpha_1 z}e^{-(t/\tau)^2}, \quad (2)$$

and in the underlayer,

$$c_2\frac{\partial\Delta T_2(z,t)}{\partial t}=K_2\frac{\partial^2\Delta T_2(z,t)}{\partial z^2}+I(1-R_1)(1-R_2)\alpha_2 e^{-\alpha_1 l}\times e^{-\alpha_2(z-l)}e^{-(t/\tau)^2}. \quad (3)$$

In these equations, c_i is the heat capacity per unit volume, $\Delta T_i(z,t)$ is the temperature change as a function of distance z and time t, K_i is the thermal conductivity, I is the laser intensity, R_i is the reflectivity of the metal surface, α_i is the absorption coefficient, l is the depth of the interface, and $i=1,2$ for the upper and lower layers, respectively. We have assumed a Gaussian temporal profile for the heating-source term, although the details of the pulse shape are unimportant for durations (τ) of a few picoseconds.[11]

The boundary conditions imposed on the temperature at the surface, the interface, and sufficiently deep in the material are given by

$$\left.\frac{\partial\Delta T_1}{\partial z}\right|_{z=0}=0, \quad (4)$$

$$\left.\frac{\partial\Delta T_2}{\partial z}\right|_{z=z_{\max}}=0, \quad (5)$$

$$\Delta T_i(z,t<-5\tau)=0, \quad (6)$$

$$\Delta T_2(z_{\max},t)=0, \quad (7)$$

$$-K_1\frac{\partial\Delta T_1(l^-,t)}{\partial z}=-K_2\frac{\partial\Delta T_2(l^+,t)}{\partial z}=[\Delta T_1(l^-,t)-\Delta T_2(l^+,t)]/\rho, \quad (8)$$

where ρ is the interfacial thermal impedance. Boundary conditions (4) and (5) stipulate negligible heat flow both out of the surface and deep in the material for the duration of our measurement. Conditions (6) and (7) indicate that for times prior to the heating pulse and for sufficient depths, there is no temperature change. The boundary condition in Eq. (8) simply expresses the conservation of thermal flux across the interface.

The heat-conduction equations (2) and (3) are solved by the method of finite differences using the DuFort-Frankel explicit approximation which is unconditionally stable.[18] Solution of these equations results in both the spatial and temporal profile of the sample temperature. By fitting our TTR measurement of the surface temperature to the calculation, we determine the thermal impedance of the interface between the two metals comprising a bilayer film. A two-parameter-fitting routine uses the thermal impedance and a constant coefficient as the free parameters. The Appendix contains a more-detailed description of the calculational procedure.

The results of the fit are sensitive to the values used for the absorption coefficient, the thickness of the top layer, and the thermal conductivity of each layer. We determine the individual layer conductivities from TTR measurements of the thermal diffusivity in separate reference films of the same elements used in the bilayers. The thermal conductivity is obtained by multiplying the measured diffusivity ($\kappa=K/c$) by the literature value of heat capacity. This assumes that any deviation in thermal diffusivity results largely from deposition-induced perturbations to the thermal conductivity.

The sensitivity of the fit to the sample absorptivity arises from the fact that the temperature decay time is on the order of $1/\alpha^2\kappa$. That is, the time required for the heat to diffuse out of the optical skin depth. We determine the sample absorptivity (α) from photometric measurements of the complex refractive index of the sample.

Although the solutions for the temporal response of the surface temperature account for the finite heating depth, we neglect depth-dependent contributions to the thermoreflectance signal. That is, we fit the calculated surface temperature profile to our TTR measurement. We expect the depth-dependent contributions to the thermoreflectance will be minor as a result of the exponential decay of both the incoming and outgoing optical fields, and the surface transmission and reflection factors. The essential features of interfacial thermal transport can be demonstrated and the added calculational complexity is not warranted.

It is clear from the preceding discussion that we are taking a very macroscopic approach to modeling the thermal transport through interfaces on the atomic scale. Certainly a rigorous treatment of transport processes begins with the Boltzmann equation, which under certain simplifications, reproduces the Fourier heat-conduction model that we use.[19] In spite of the apparent loss of microscopic detail, this treatment of thermal transport in solids has been successfully applied to numerous problems. Our only justification for using this approach is founded on the intuitive clarity of the model and the boundary conditions. We caution, however, that the details of electron scattering from the interfacial lattice potential are lost in our model. Nevertheless, the experimental approach reveals the physics of interfacial thermal transport, and we believe our measurements could be subjected to a more rigorous analysis.

III. APPARATUS AND SAMPLE PREPARATION

Our experimental apparatus consists of two synchronously pumped dye lasers which generate 4-psec pulses at a wavelength of 633 nm for the heating pulse and 595 nm for the probe pulse. An adjustable delay line is used to increment the time delay of the probing pulse relative to the heating pulse. The position of zero time delay is determined by performing a cross-correlation measurement of the two laser pulses interacting in a nonlinear optical crystal placed in the sample position. The average heating and probing laser power at the sample is 50 and 2 mW, respectively.

Although we are performing a time-resolved measurement, the detection scheme is quasicontinuous. Because the laser-pulse repetition rate is 246 MHz, we can amplitude modulate the heating-pulse train at 10 MHz. The thermomodulation of the reflected probe-pulse train is retrieved by a lock-in amplifier tuned to the modulation frequency. This TTR signal is measured as a function of the time delay of the probe pulses relative to the heating pulses.[11,20]

The heating-pulse energy of 0.2 nJ is focused within a diameter of roughly 20 μm. Depending on the material reflectivity and heat capacity, typical surface temperature increases are on the order of 10 K in metals. This results in a fractional reflectivity change of $\sim 10^{-5}$, and the detection limit of our system is 10^{-7}. With such small temperature increases and reflectivity changes, perturbations to the material properties are negligible.

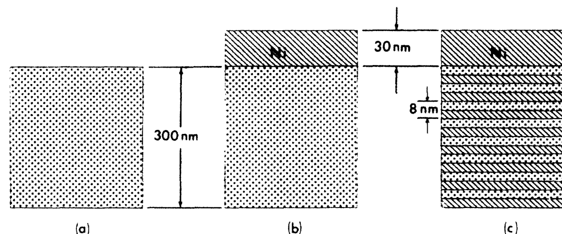

FIG. 1. Sample geometry: (a) single-element film; (b) bilayer film; (c) multilayer film. Both the bilayer and multilayer films are capped with 30 nm of Ni.

Samples were prepared in a dual-source magnetron sputter deposition system with a base pressure below 1×10^{-7} Torr. Oxidized silicon wafers and Kapton (for transmission x-ray diffraction) were coated simultaneously. Sequential deposition of metal pairs was achieved by rotating the substrates under the simultaneously operating, shielded sputter sources. Deposition rates were held constant at 5 Å/sec and the sputtering atmosphere was 2 mTorr of argon.

The bilayer samples consisted of a 30-nm Ni cap deposited over a 300-nm-thick underlayer. The underlayer metals used were Cu, Mo, Ti, and Zr. In addition, 300-nm-thick single-element films were fabricated using the same deposition conditions. These samples provided reference values for the thermal diffusivities of the bilayer constituents.

Multilayers of the same metal pairs were prepared by continuous rotation of the substrates under the sources. Since the deposition rates of the two sources were the same, equal thicknesses of each metal were deposited. The rotation rate of the sample substrate was set to produce a composition modulation wavelength (Λ) of 8 nm. Multilayer films were deposited to a total thickness of 300 nm, with a 30-nm Ni cap on top. The Ni cap serves as an optically thick heating source and thermoreflectance transducer. The geometry of the various sample structures is shown in Fig. 1.

IV. OPTICAL PROPERTIES

As previously noted, the TTR measurement of thermal diffusivity requires an accurate value for the optical-absorption coefficient of the sample. The coefficient α can be calculated using the relation $\alpha = 4\pi k/\lambda$, where λ is the incident wavelength and k is the imaginary part of the complex refractive index $(n+ik)$.[21]

The sample refractive index is determined from the ratio of the reflectivities for s-polarized and p-polarized light at a wavelength of 633 nm (the heating laser wavelength). The reflectivity ratio is measured at both 30° and 70° angles of incidence, and the refractive index is

TABLE I. Optical properties of the single-element, bilayer, and multilayer films.

Sample		n	k	α (10^7 m^{-1})
Single element	Ni	1.80	3.71	7.4
	Mo	3.07	3.84	7.6
	Ti	2.77	3.64	7.2
	Zr	2.33	3.69	7.3
Bilayer film	Ni-Cu	1.73	3.70	7.3
	Ni-Mo	1.80	3.85	7.6
	Ni-Ti	1.63	3.54	7.0
	Ni-Zr	1.81	3.80	7.5
Multilayer film	Ni-Cu	1.77	3.76	7.5
	Ni-Mo	1.50	3.27	6.5
	Ni-Ti	1.78	3.76	7.5
	Ni-Zr	1.60	3.45	6.9

determined by fitting our measurement to the appropriate Fresnel formulas.[22] The measured optical properties of the samples are listed in Table I.

As in any photometric measurement, the results can be sensitive to surface oxidation and contamination.[23] The variation in the Ni refractive index probably results from oxidation and error in our measurement. We attempt to minimize these problems by performing repeated measurements on the samples immediately after removal from the deposition chamber. With the exception of Ti, we find that our measured value for k is within 10% of the literature value[21] for the single-element films.

An accurate measurement of refractive index would require ultrahigh vacuum conditions and clean sample surfaces. However, we believe our current accuracy in determining the film absorptivity is sufficient to permit a relative comparison of thermal transport in the various samples. By depositing Ni overlayers on both the bilayer and multilayer samples, we avoid gross inconsistencies in surface optical properties, and the essential features of thermal transport can be observed and interpreted on sound physical grounds.

V. X-RAY DIFFRACTION MEASUREMENTS

The structural order of metal-metal interfaces is very sensitive to the atomic size mismatch between the constituent elements. For Ni-metal interfaces, the size mismatch increases in the order Ni-Cu, -Mo, -Ti, -Zr.[12] In an isostructural system with small mismatch, such as Ni-Cu, coherent interfaces are produced and some interdiffusion is expected. In the case of Ni-Mo, there exists a possibility of epitaxial alignment of rows of atoms in the fcc Ni(111) and the bcc Mo(110) planes;[24] crystalline superlattices have been observed.[25] Although the mating planes of Ni-Ti and Ni-Zr have the same symmetry [Ni:fcc(111) and Ti,Zr:hcp(001)], there exists a rather large size mismatch of $\sim 15\%$ in Ni-Ti and $\sim 26\%$ in Ni-Zr. There is no structural information transmitted from layer to layer, and there is experimental evidence for an amorphous interfacial layer which is

TABLE II. Summary of the x-ray diffraction results for the sample films. The orientation of Zr and Ti in the single-element and bilayer films is a combination of (100) and (001) structures; the number given is the relative fraction of these two orientations contained in the film.

Sample type	Element	Orientation	Homogeneous strain (%)	Inhomogeneous strain (%)	Domain size (nm)
Single element	Zr	(100)/(001) 4.0	0.7/1.5	0.6/0.9	56/53
	Ti	(100)/(001) 0.23	0.5/0.8	0.1/1.1	23/74
	Mo	ω(110)	1.0	0.7	50
	Ni	ω(100)	0.3		
Bilayer	Zr	(100)/(001) 3.2	0.7/1.6	0.6/0.0	85/21
	Ni	(111)	0.1	0.0	16
	Ti	(100)/(001) 0.19	0.5/0.9	0.4/1.2	30/130
	Ni	(111)	0.1	0.6	30
	Mo	ω(110)	0.7	1.0	90
	Ni	random	0.3		
	Cu	random	0.5		
	Ni	random	0.1		
Multilayer	Zr	(001)			
	Ni	(111)			
	Ti	(001)			
	Ni	(111)			
	Mo	(110)			
	Ni	(111)			
	Cu	random			
	Ni	random			

larger in Ni-Zr than in Ni-Ti.[26,27]

The structure of our samples was investigated by x-ray diffraction in both reflection and transmission geometries. This permits a differentiation between samples with and without strong crystal orientation texture. In addition, orientation texture was investigated by rocking-curve measurements and by relative peak intensities which were corrected for Lorentz-polarization, temperature, thickness, structure, and multiplicity adjustments.[28] Homogeneous strain was deduced from diffraction peak shifts, and the peak widths were used to gain information on crystal size and inhomogeneous strain.[29]

The result of the x-ray diffraction analysis are summarized in Table II. In the single-element and bilayer films, the hcp metals Ti and Zr exhibit both (100) or (001) orientations, with Zr showing more (100) and Ti more (001). The deduced strain and domain size are different for each orientation. In the single-element and bilayer films, Mo shows a weak (110) orientation. The single-element Ni film was deposited in 30-nm layers to duplicate the deposition conditions of the Ni cap on the bilayer samples. This produced a weak (100) orientation in the single-element film.

The Ni overlayer orientation was found to be dependent on the underlayer metal. A Ni(111) orientation occurred on both the Ti and Zr bilayer films, while no preferred orientation was observed to occur on the Mo or Cu underlayers. This influence of the underlayer on the overlayer growth can be explained by considering the interfacial structure. In the case of the Mo and Cu, the ability to form coherent interfaces with Ni results in a propagation of the underlayer structure into the overlayer. Thus the weakly oriented Mo and Cu can lock the thin Ni overlayer into a random orientation. On the other hand, the Ni-Zr and Ni-Ti interfaces are incoherent, and the Ni overlayer can relax into a lower-energy configuration during growth away from the interface.

The effect of orientation and strain on thin-film thermal properties is not well known. It is likely that inhomogeneous strain will result in a lower thermal diffusivity due to electron scattering from lattice distortions. Grain boundaries will also act as scattering sites,[30] and we expect that relatively smaller domain sizes will degrade thermal diffusion. Because we use the measured thermal properties of the single-element films to deduce the interfacial impedance in the bilayer films, it is unfortunate that the Ni overlayer structure is sensitive to the underlayer. However, the structure of the Ti and Zr is the same in both the bilayer and the single-element films. This will allow us to demonstrate the influence of interfacial structure on thermal transport in these samples.

Figure 2 shows the small-angle diffraction data for the Ni-Cu, Ni-Mo, Ni-Ti, and Ni-Zr multilayer samples. In each case, sharp peaks are observed which can be used to find the composition modulation wavelength from the equation

$$\sin^2\theta=(\lambda/2\Lambda)^2 n^2+2\delta \ , \quad (9)$$

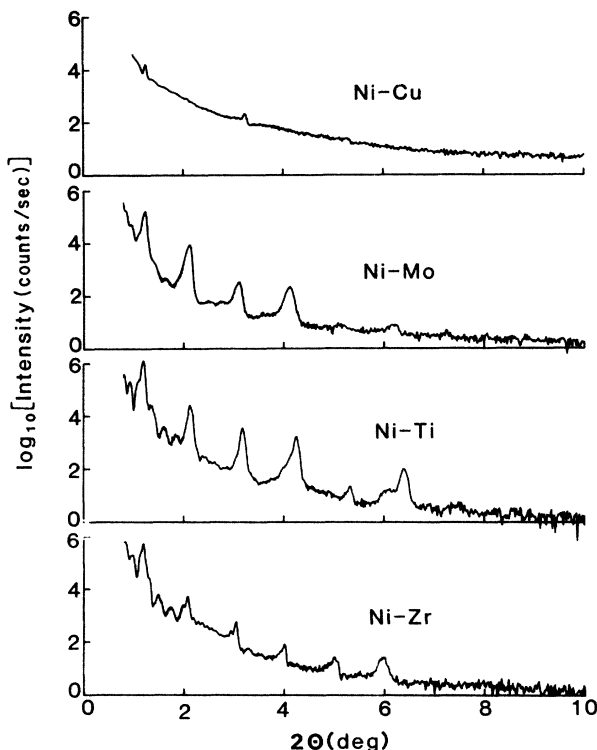

FIG. 2. Small-angle reflection x-ray diffraction for the multilayer samples.

where θ is the observed scattering angle for a diffraction peak, λ is the radiation wavelength ($\lambda_{\mathrm{Cu}\,K\alpha}=0.154\,18$ nm), Λ is the composition modulation wavelength, n is the diffraction peak order, and δ is the deviation from unity of the x-ray refractive index.[31] We find that the measured composition modulation wavelength Λ is within 10% of the design value for the multilayer films.

With the exception of Ni-Cu, all of the multilayer films are oriented with close-packed planes parallel to the sample surface. The Ni-Cu multilayer exhibited both the (111) and (200) diffraction peaks, indicating a random orientation.

In multilayer films, x-ray diffraction from the regularly spaced constituent layers can result in "satellite" peaks which accompany the main lattice diffraction peaks. However, the observation of these peaks in high-angle diffraction is strongly influenced by interfacial structure. This can be understood by considering the effect of interface structure on the statistics of layer-thickness fluctuations.[32] In the case of disordered or amorphous interfaces, the layer-thickness distribution in a multilayer will be continuous. This continuous fluctuation in layer thickness will increase the width of the high-angle diffraction peaks and eliminate the satellite peaks. On the other hand, a coherent interface will constrain a given layer thickness to be an integer number of atomic plane spacings, resulting in a discrete layer-thickness distribution. This distribution will not produce as rapid of an increase in the diffraction peak width, and consequently the satellite peaks will persist with much larger layer-thickness fluctuations.

Figure 3 demonstrates this effect on the high-angle

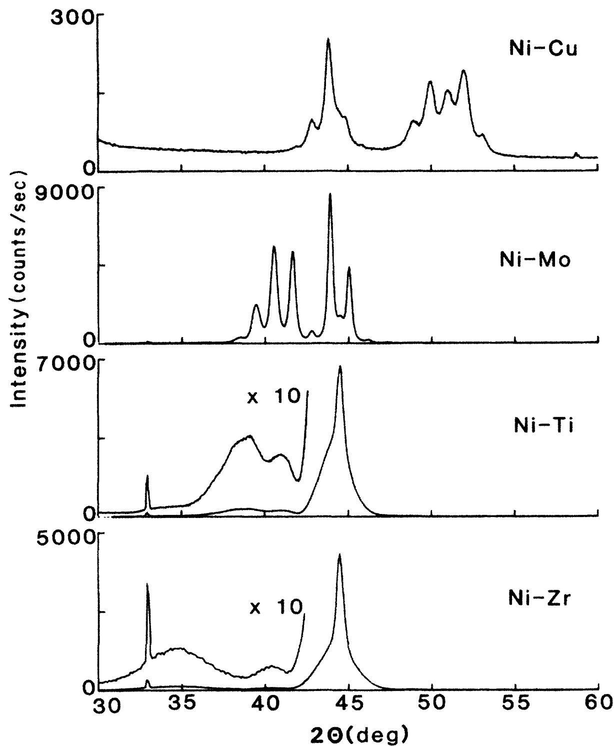

FIG. 3. High-angle reflection x-ray diffraction for the multilayer samples.

diffraction from our multilayer samples. Both the Ni-Cu and Ni-Mo samples exhibit lattice diffraction peaks accompanied by the compositional modulation satellite peaks, indicating atomic registry at the interfaces. In the case of Ni-Zr and Ni-Ti, the presence of disordered interfaces results in broad diffraction peaks which are characteristic of scattering from independent layers of the constituent elements. No diffraction satellites are observed from these multilayer films.

VI. THERMAL DIFFUSIVITY

The thermal impedance of the bilayer interface is found by fitting the simultaneous solution of Eqs. (2) and (3) to the TTR measurement. In order to obtain a unique value for the impedance, the thermal conductivities of the individual metal films are required input parameters. As previously noted, these values are obtained from TTR measurements on the single-element films which were fabricated under the same deposition conditions as the bilayer films.

Figure 4 shows the TTR measurements for the Ni, Mo, Ti, and Zr films, and the fit thermal diffusivities are tabulated in Table III.[11] We find a substantial reduction (nearly fivefold) in the sputtered film diffusivities relative to the literature values for bulk diffusivities.[33] A reduction in transport properties is expected as a result of deposition-induced disorder in the films.[11] Although the diffusivity values are sensitive to error in the measured optical absorptivity of the films, we find that the relative values are in agreement with literature values. That is, the thermal diffusivity of Mo is the largest, followed in decreasing order by Ni, Zr, and Ti. A measurement of the Cu diffusivity was not possible due to nonequilibrium electron-heating perturbations to the TTR signal.[20]

TABLE III. The measured thermal diffusivities of the sample films.

Sample		κ (10^{-6} m^2/sec)
Single element	Ni	4.4
	Mo	13
	Ti	1.4
	Zr	2.5
Bilayer film	Ni-Cu	32
	Ni-Mo	6.1
	Ni-Ti	0.42
	Ni-Zr	0.33
Multilayer film	Ni-Cu	6.6
	Ni-Mo	1.7
	Ni-Ti	0.40
	Ni-Zr	0.40

Figure 5 compares the TTR measurements for the four bilayer films Ni-Cu, Ni-Mo, Ni-Ti, and Ni-Zr. An effective thermal diffusivity is determined in the same manner as that for the single-element films,[11] and these results are shown in Table III as well. The rate of thermal diffusion in the bilayer films is determined by both the thermal diffusivities of the individual layers as well as the interface thermal impedance.

The thermal diffusivity of Cu is greater than that of the other underlayer metals, and the large diffusivity of the bilayer film is expected on this basis. In addition, the lattice mismatch between the Ni and Cu layers is relatively small and the lattice periodicity will deviate little across the interface region. Thus, we would expect a high thermal conductance across the interface. For similar reasons, the Ni-Mo bilayer film exhibits the second largest diffusivity. This is expected due to the relative thermal diffusivity of Mo, as well as the possibility for coherent interface structure. In the limit of inter-

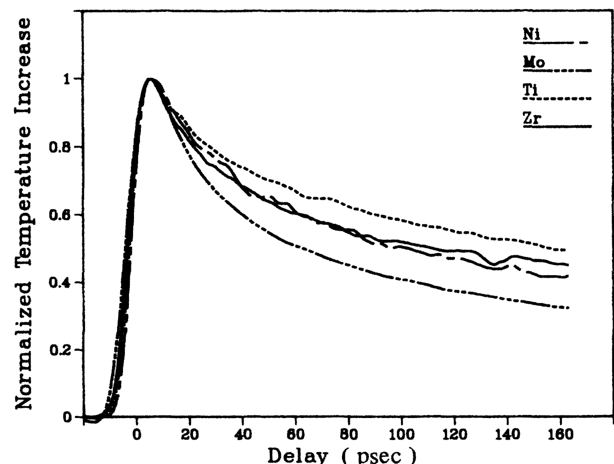

FIG. 4. Transient thermoreflectance (TTR) measurements of the single-element films.

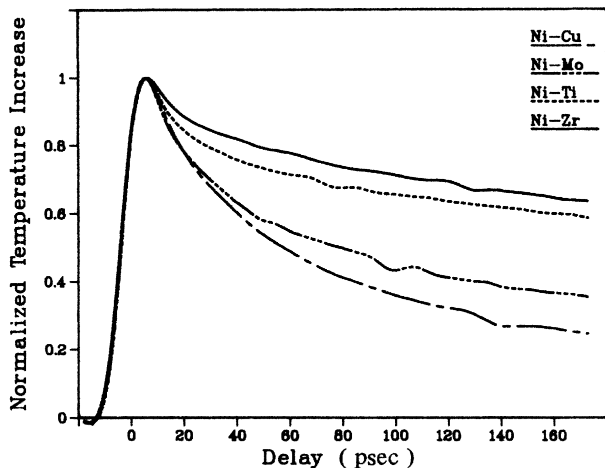

FIG. 5. TTR measurements of the bilayer films.

facial epitaxy, scattering of electrons between Fermi momentum states on either side of the interface would be mediated by the contact potential barrier.[12] Thus the measurement of this intrinsic thermal barrier in epitaxial systems could provide information about the contact potential.

The effect of interface impedance is most apparent in the Ni-Ti and the Ni-Zr films. Although the measured thermal diffusivity of the Zr is greater than that of Ti, we find the effective thermal diffusivity of the Ni-Ti bilayer to be larger than that measured for Ni-Zr. We attribute this result to the presence of a larger interface impedance in the Ni-Zr bilayer relative to the Ni-Ti bilayer. This is consistent with the observation of more interfacial disorder in multilayers of Zr-Ni relative to Ti-Ni.[26] The larger heat of mixing and atomic diffusivity of Ni in Zr result in a larger amorphous region in Zr-Ni than in Ti-Ni. This causes an extended disruption of the lattice potential and leads to more diffuse scattering of the hot conduction electrons. Our observations indicate that this interfacial scattering can indeed dominate thermal transport through metal systems, in spite of the absolute transport properties of the constituents.

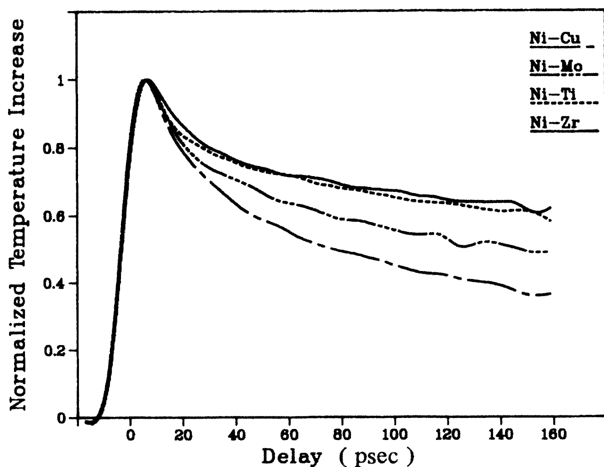

FIG. 6. TTR measurements of the multilayer films.

The TTR measurements of the four multilayer films are shown in Fig. 6. The relative order of the temperature decay in these films is the same as that exhibited for the bilayer films. In the case of the Ni-Ti and Ni-Zr multilayers, however, the fit thermal diffusivities are equal. This occurs because we measure a lower absorption coefficient in the Ni-Zr relative to the Ni-Ti. Consequently, the apparent optical heating depth is larger in the Ni-Zr and more time is required for diffusion out of the heated layer. Table III contains the effective thermal diffusivities which were obtained by using our fitting procedure and the measured optical properties from Table I.

VII. INTERFACE THERMAL IMPEDANCE

Our initial characterization of the bilayer films by an effective thermal diffusivity is useful for demonstrating the decrease in thermal transport resulting from a metal-metal interface. However, our goal is to apply the two-layer model of thermal transport to the bilayer measurements in order to obtain values for the interface thermal impedance. Using Eqs. (2) and (3) and the numerical procedure discussed in the Appendix, we have fit the Ni-Ti measurement as shown in Fig. 7. The fit yields a value for the interfacial thermal impedance ρ defined by the boundary condition of Eq. (8). Our results for both the Ni-Ti and Ni-Zr bilayer films are tabulated in Table IV. We have also included the relative lattice mismatch for the metal pairs, as determined from literature values of lattice constants for the appropriate crystal orientations.[12]

In the case of the Ni-Cu and Ni-Mo bilayers, our numerical analysis failed to converge on consistent values for the interfacial impedance. Equally accurate fits could be obtained with a range of impedance values which were several orders of magnitude smaller than those obtained for Ni-Ti and Ni-Zr. This indicates that the thermal impedances of the Ni-Mo and Ni-Cu interfaces are relatively negligible and thermal diffusion is

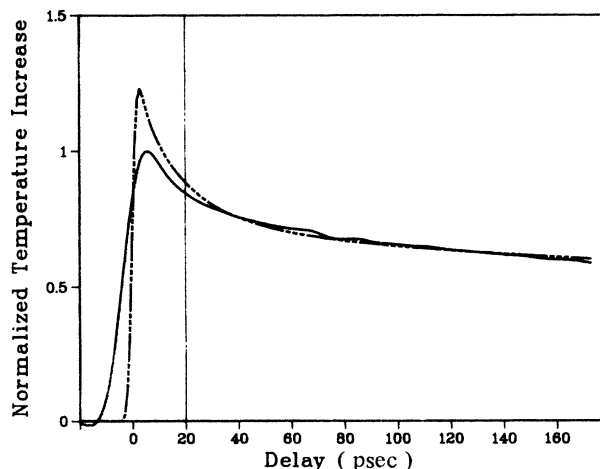

FIG. 7. TTR measurement of the Ni-Ti bilayer film and the best-fit solution (broken line) of the heat-flow model which yields the interface impedance.

TABLE IV. The measured thermal impedance of the bilayer film interface. The lattice mismatch is the fractional deviation in nearest-neighbor distances between the mating planes of the Ni overlayer and the various underlayer elements (relative to Ni).

Sample	Lattice mismatch (%)	Interfacial thermal impedance (ρ) (10^{-9} m^{2}K/W)
Ni-Cu	2.8	
Ni-Mo	9.2	
Ni-Ti	16.1	1.9
Ni-Zr	27.3	2.3

dominated by the Cu and Mo underlayers.

We have found that the values obtained for the interface impedance are sensitive to the overlayer thickness and the constituent thermal conductivities used as input parameters. Although we have not performed a detailed sensitivity analysis at this point, we believe the values in Table IV are semiquantitative at best. For instance, we have found that a 10% error in the overlayer film thickness can double the value obtained for the thermal impedance. The exaggerated parameter sensitivity and nonconvergence problems of our model very likely result from an oversimplified approach to the thermal transport and the numerical analysis. Nevertheless, our preliminary tests of the fitting procedure consistently yield a smaller impedance value for the Ni-Ti interface relative to the Ni-Zr interface. Without question, our experimental observations demonstrate the impedance of thermal transport by a metal-metal interface and the influence of interfacial disorder.

VIII. DISCUSSION

Having reviewed our TTR measurements of thermal transport in all of the films, it is instructive to compare the results for each metal pair. Figure 8 shows the TTR measurements for the Ni, Ti, Ni-Ti bilayer and Ni-Ti multilayer films. Comparing the bilayer-film and the single-element-film measurements, we can readily observe the degradation in thermal diffusion which results from the presence of a single interface. As shown in Fig. 9, this effect is also observed in the Ni-Zr bilayer relative to the Ni and Zr data.

It is interesting to note that the multilayer Ni-Ti film has approximately the same thermal diffusivity as the bilayer film. Even more surprising is the result that the Ni-Zr multilayer has a greater thermal diffusivity than the Ni-Zr bilayer. In light of the rather dramatic effect of a single interface, one might expect that the presence of several interfaces would severely impede thermal transport. However, we must consider the fact that in the multilayer film, one-half of the 300-nm underlayer is composed of Ni, which has a larger thermal diffusivity than either Ti or Zr.

In order to examine this effect, we construct a simple model to calculate the effective thermal conductance of a multilayer structure. We model the effective thermal impedance within a composition modulation wavelength (8 nm) as a series combination of the individual layer impedances and the interface impedance. This is a reasonably valid model when the electron mean free path is much less than the layer thickness (4 nm) or when the interfacial scatter is diffuse. Under these conditions the electrons acquire a drift velocity within the thermal gradient of each layer, and if the scattering at the interface is diffuse, each electron crossing the interface loses memory of its prior velocity. As a result, the layers can be treated as separate impedances connected in series by the interface impedance. This series impedance model is appropriate for the one-dimensional thermal transport which we are probing.

Considering the substantial transport reduction observed in the Zr and Ti films relative to bulk values, mean free paths less than the 4-nm unit distance (one-

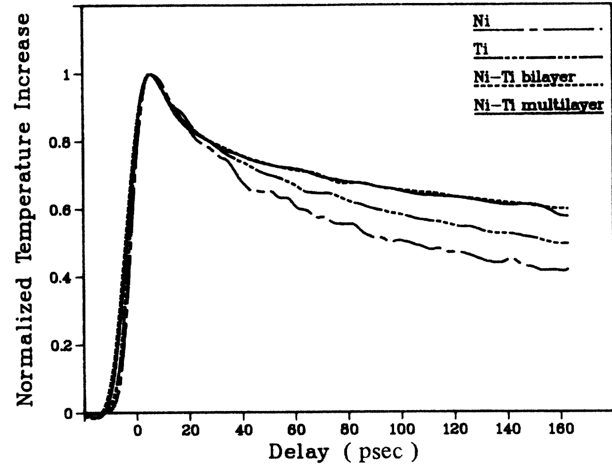

FIG. 8. TTR measurements demonstrating the relative thermal transport in the Ni, Ti, Ni-Ti bilayer and multilayer films. The presence of a single interface is responsible for the reduced thermal transport in the bilayer film relative to the single-element films. The additional Ni present in the multilayer film compensates for the thermal impedance of the multiple interfaces.

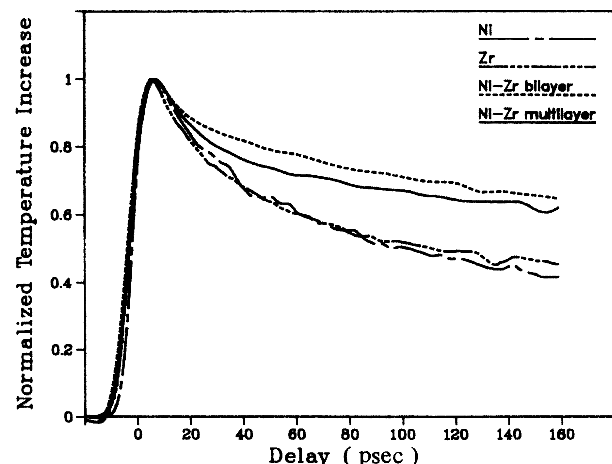

FIG. 9. TTR measurements of the Ni, Zr, Ni-Zr bilayer and multilayer films.

half the modulation wavelength) are expected in the bilayer films.[34] Furthermore, in the multilayer films the disordered interface region will diffusely scatter electrons and establish a 4-nm upper limit on the mean free path. For a multilayer film with individual layer thicknesses t, the effective multilayer thermal conductivity is given by

$$K_m = [\tfrac{1}{2}(1/K_u + 1/K_0) + \rho/t]^{-1} , \qquad (10)$$

where ρ is the interface impedance from Eq. (8) and K_o and K_u are the over- and underlayer constituent conductivity. Using our measured values of κ (Table III) and handbook values for the heat capacity, we calculate K_u and K_o. Inserting these values and the measured value for ρ into Eq. (10), we find that the calculated value of the Ni-Ti multilayer thermal conductivity K_m is about one-half of the thermal conductance K_u of Ti; K_m for Ni-Zr is about one-third of K_u for Zr. Thus, despite the large number of thermally resistive interfaces, the thermal conductivity of the multilayer is not expected to be much smaller than that of the poorest thermal conducting constituent.

The situation is different when the underlayer metal (Mo,Cu) has a thermal diffusivity which is larger than that of the Ni overlayer. In Fig. 10 we see that the Ni-Mo bilayer signal falls between that of the Ni and Mo, indicating that the interface impedance is small relative to the incremental impedance of Ni. However, it is not entirely negligible, as demonstrated by the observation that the multilayer Ni-Mo film has a diffusivity smaller than that of Ni. Figure 11 shows that both the Ni-Cu bilayer and multilayer have diffusivities exceeding that of Ni, indicating that the Ni-Cu interface impedance is negligible.

IX. CONCLUSIONS

In the preceding discussion we have qualitatively interpreted our observations of thermal transport in the various metal pairs. To some extent we have ignored the microscopic details of the structural differences in the reference and bilayer films, and we have attempted a

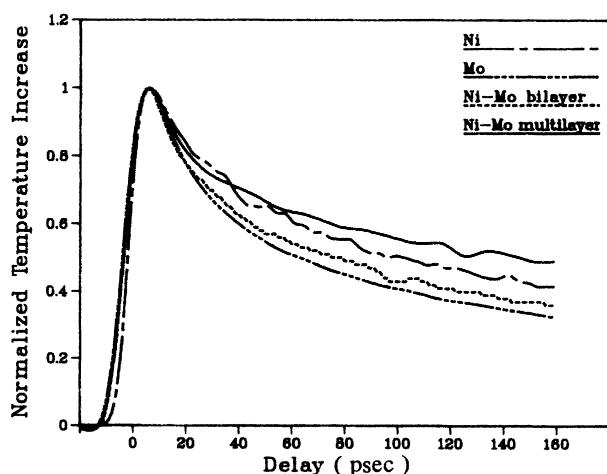

FIG. 10. TTR measurements of the Ni, Mo, Ni-Mo bilayer and multilayer films.

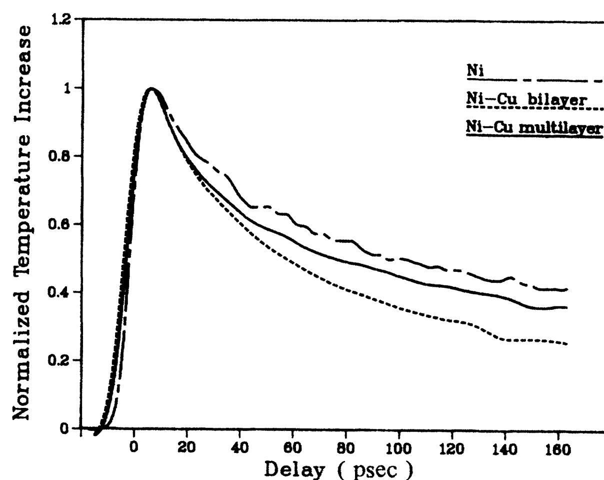

FIG. 11. TTR measurements of the Ni, Ni-Cu bilayer and multilayer films.

quantitative comparison of the various samples. Ideally, the crystal orientations observed in the single-element films would be preserved in the bilayer and multilayer films. However, the underlayer orientation can have a strong influence on the growth of an overlayer, and as a result the structure of the bilayer films can be different from the reference and multilayer films. Although the thermal conductivity of a metal depends weakly on orientation, we expect the most dramatic influence of orientation will be found at the interface between two different metals. It is the crystal structure of the contacting metal pairs which determines the degree of interfacial coherence.

Fully quantitative results would require the structure of the single-element reference films to be the same as that of the layered single-element components. In our study, a serious consideration occurs in the case of the Ni film where we find the structure varies from weak (100) orientation to (111) on Ti and Zr, and random structure in the Cu and Mo multilayers. The most conspicuous example of changing orientation is in Ni-Zr (see Table II), where we find that the Zr orientation alters from (100) to (001) in going from the bilayer to the multilayer film. It is conceivable that if the multilayer Zr were oriented along the (100) direction as in the bilayer film, then the multilayer diffusivity may not exceed that of the bilayer film (see Fig. 9). This conjecture illustrates the point that a fully consistent comparison of the results is not possible.

In spite of our concerns regarding sample consistency and the numerical analysis sensitivities, we believe we have provided a physically consistent explanation of the observed thermal transport in these particular metal-metal systems. We have investigated four metal pairs which exhibit a systematic variation in lattice mismatch and interfacial coherence. This has permitted us to observe the dramatic influence interfacial disorder has on thermal transport in metals.

These measurements are made possible by a novel one-dimensional thermal transport probe which is based on the thermally-induced change in surface reflectivity. With refinements in numerical analysis and sample

preparation, these measurements should be capable of providing fully quantitative studies of thermal transport in thin films. We expect this measurement technique will also impact on investigations of size effects and grain-boundary impedances. In the event that the electrical and thermal transport are related by a proportionality constant (Lorenz number[12]) the electrical transport properties can be inferred from the thermal transport measurements. This is especially important because the TTR measurement is noncontacting and one dimensional.

In addition to our studies of thermal transport in metal-metal systems, we have observed the generation and propagation of picosecond duration acoustic pulses.[35] The acoustic pulse echoes, which reflect from the film-substrate interface, produce a transient piezoreflectance signal which accompanies the thermoreflectance transient. A measurement of the acoustic velocity is straightforward, and this overall capability to study both the transport and elastic properties of thin-film materials provides a powerful new tool.

ACKNOWLEDGMENTS

The authors would like to thank William H. Frey for his help in the development of the computer program for calculating the thermal impedance.

APPENDIX

Equations(2) and (3) can be rewritten in finite difference form using the DuFort-Frankel explicit approximation as

$$c_i\left[\frac{T_k^{j+1}-T_k^{j-1}}{2\Delta t}\right]=K_i\left[\frac{T_{k+1}^{j}-T_k^{j+1}-T_k^{j-1}+T_{k-1}^{j}}{(\Delta z)^2}\right]+Q_{i,k}^{j+1}\ , \qquad \text{(A1)}$$

where subscript i denotes the layer index, and subscripts j and k represent a step in time (Δt) and distance (Δz), respectively. The forcing function for each layer is denoted as Q, where

$$Q_{1,k}^{j+1}=I(1-R)\alpha_1 e^{-\alpha_1(k-1)\Delta z}e^{-[t_0+(j-1)\Delta t/\tau]^2}\ , \qquad \text{(A2)}$$

for the top metallic layer and for the underlayer

$$Q_{2,k}^{j+1}=I(1-R_1)(1-R_2)\alpha_1 e^{-\alpha_1 l}e^{-\alpha_2[(k-1)\Delta z-l]}\times e^{-[t_0+(j-1)\Delta t/\tau]^2} \qquad \text{(A3)}$$

The DuFort-Frankel approximation can have a smaller error than the classical explicit method and is also unconditionally stable, thereby allowing larger values of Δt.[18] There is, however, a limit on the ratio $\Delta t/\Delta z$ given by consistency considerations. Figure 12 shows graphically the DuFort-Frankel approximation scheme.

The interfacial boundary condition can be written in difference form as

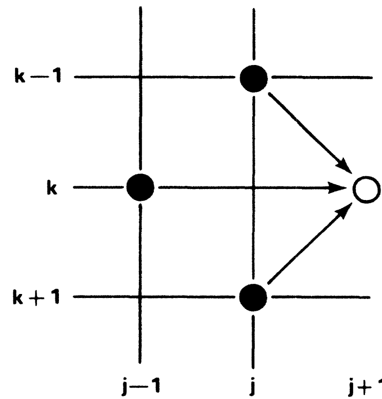

FIG. 12. Graphical representation of the DuFort-Frankel numerical method for solving the heat diffusion equation. The distance and time indices are represented by k and j, respectively.

$$-\frac{K_1}{\Delta z}(T_{-1}^{j+1}-T_{-2}^{j+1})=-\frac{K_2}{\Delta z}(T_1^{j+1}-T_0^{j+1})=(T_{-1}^{j+1}-T_0^{j+1})/\rho\ . \qquad \text{(A4)}$$

Solving for T_{-1}^{j+1}, and T_0^{j+1}, the temperature at the nodes immediately above and below the metal-metal interface, respectively, gives

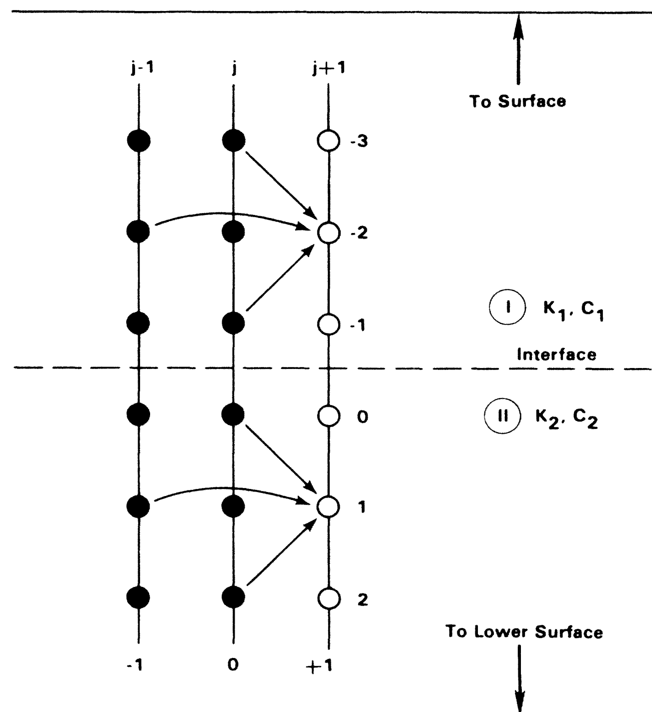

FIG. 13. Graphical representation of the numerical method in the vicinity of the interface between thermally different materials. Equations (A5) and (A6) are used to calculate the temperatures on either side of the interface ($k=0,-1$).

$$T_{-1}^{j+1}=\frac{T_1^{j+1}(K_2\Delta z/\rho)+T_{-2}^{j+1}[K_1(K_2+\Delta z/\rho)]}{K_1K_2+\Delta z(K_1+K_2)/\rho} \quad (A5)$$

and

$$T_0^{j+1}=\frac{T_1^{j+1}[K_2(K_1+\Delta z/\rho)]+T_{-2}^{j+1}(K_1\Delta z/\rho)}{K_1K_2+\Delta z(K_1+K_2)/\rho} . \quad (A6)$$

Figure 13 shows the graphical representation of the finite-difference scheme in the vicinity of the interface. The solution for the temperature T_k^{j+1} is generated by starting the calculation very deep in the underlayer and solving for all mesh points up to the surface except for T_{-1}^{j+1} and T_0^{j+1}, the nodes directly adjacent to the interface. The temperature at these points is determined using Eqs. (A5) and (A6). If these two mesh points are not treated symmetrically about the interface the calculation becomes unstable.

A uniform temporal mesh was used for the entire calculation in order to satisfy the accuracy and convergence criteria of the calculation. The temporal mesh size was approximately $3\times10^{-3}\tau$ and the total number of temporal nodes for the calculation was on the order of 30 000. A uniform spatial mesh was used for the calculation from 10 Å below the interface up to the surface. The mesh size in this region was 0.5 Å. Below the interface the thermal gradient is no longer changing rapidly and therefore a wider spatial mesh can be utilized. The mesh was refined in this region using a geometric progression so that less than 650 nodes were used to take the calculation 2.5 μm into the sample.

The spatially nonsymmetric difference formula can be simplified as

$$T_k^{j+1}=\left[\frac{1-\omega}{1+\omega}\right]T_k^{j-1}+\left[\frac{2\omega}{1+\omega}\right]\times[\gamma T_{k+1}^{j}+(1-\gamma)T_{k-1}^{j}]+\sigma_k^{j+1} , \quad (A7)$$

where Δ_k is the kth spatial increment,

$$\sigma_k^{j+1}=\frac{2Q_k^{j+1}\Delta t}{c_i+2K_i\Delta t/\Delta_k\Delta_{k+1}} , \quad (A8)$$

$$\gamma=\frac{\Delta_k}{\Delta_k+\Delta_{k+1}} , \quad (A9)$$

$$\delta=\tfrac{1}{2}(\Delta_k+\Delta_{k+1}) , \quad (A10)$$

$$\omega=\frac{K_i\Delta t}{2c_i\gamma(1-\gamma)\delta^2} . \quad (A11)$$

Our fitting routine begins with seed values for the interfacial impedance, ρ, and the overall scaling factor which matches the amplitude of the data to the calculated surface temperature profile. The Simplex[36] fitting routine then adjusts the seed values in a direction which minimizes the mean-square difference between the solution of Eq. (A7), (A6), and (A5) and the TTR profile. The fitting routine is more sensitive to the optical-absorption coefficient, the upper layer thickness, and the thermal conductivity of the two layers than it is to the interfacial impedance or the overall scaling factor. This was exhibited by altering the routine to fit each of these parameters separately for a fixed ρ. In each case the convergence was more rapid than that for determining ρ, but the least-squares difference remained approximately the same.

---

*Present address: IBM Corporation, 1701 North Street, Endicott, NY 13760.

[1] *Proceedings of the Yamada Conference XIII on Electronic Properties of Two-Dimensional Systems (Kyoto, Japan, 1985),* edited by T. Ando [Surf. Sci. **170** (1986)].

[2] *Synthetic Modulated Structures,* edited by L. Cheng and B. C. Giessen (Academic, New York, 1985).

[3] I. K. Schuller and C. M. Falco, in *VLSI Electronics: Microstructure Science,* edited by N. Einspruch (Academic, New York, 1982), Chap. 5.

[4] *Dynamical Phenomena at Surfaces, Interfaces and Superlattices,* edited by F. Nizzoli, K. Rieder, and R. Willis (Springer-Verlag, Berlin, 1985).

[5] C.-X. Chen, Appl. Phys. A **40**, 37 (1986).

[6] C.-X. Chen, Appl. Phys. A **42**, 145 (1987).

[7] M. Gurvitch, Phys. Rev. B **34**, 540 (1986).

[8] T. R. Werner, I. Banergee, Q. S. Yang, C. M. Falco, and I. K. Schuller, Phys. Rev. B **26**, 2224 (1982).

[9] P. F. Carcia and A. Suna, J. Appl. Phys. **54**, 2000 (1983).

[10] G. Bergman, Phys. Rev. B **19**, 3933 (1979).

[11] C. A. Paddock and G. L. Eesley, J. Appl. Phys. **60**, 285 (1986).

[12] N. W. Ashcroft and N. D. Mermin, *Solid State Physics* (Holt, Rinehart and Winston, New York, 1976).

[13] M. Cardona, *Modulation Spectroscopy* (Academic, New York, 1969).

[14] K. Ujihara, J. Appl. Phys. **43**, 2376 (1972).

[15] M. V. Iravani and H. K. Wickramasinghe, J. Appl. Phys. **57**, 122 (1985).

[16] J. Baker-Jarvis and R. Inguva, J. Appl. Phys. **57**, 1569 (1985).

[17] D.L. Balageas, J. C. Krapez, and P. Cielo, J. Appl. Phys. **59**, 348 (1986).

[18] L. Lapidus and G. F. Pinder, *Numerical Solutions of Partial Differential Equations in Science and Engineering* (Wiley, New York, 1982).

[19] M. J. Mauer, J. Appl. Phys. **40**, 5123 (1969).

[20] G. L. Eesley, Phys. Rev. B **33**, 2144 (1986).

[21] *Physics Data: Optical Properties of Metals,* edited by J. H. Weaver, C. Krafka, D. W. Lynch, and E. E. Kock, (Fachinformationszentrum, Karlsruhe, Federal Repubic of Germany, 1981).

[22] R. H. Huebner, E. T. Arakawa, R. A. McRae, and R. N. Hamm, J. Opt. Soc. Am. **54**, 1434 (1964).

[23] L. Ward, Opt. Laser Tech. **17**, 263 (1985).

[24] E. Bauer and Jan H. van der Merwe, Phys. Rev. B **33**, 3657 (1986).

[25] I. K. Schuller, Phys. Rev. Lett. **44**, 1597 (1980).

[26] B. M. Clemens, Phys. Rev. B **33**, 7615 (1986).

[27] B. M. Clemens, J. Appl. Phys. **16**, 4525 (1987).

[28] B. D. Cullity, *Elements of X-Ray Diffraction* (Addison-

Wesley, Reading, MA, 1967).
[29]S. F. Bartram, in *Handbook of X-Rays,* edited by E. F. Kaelble (McGraw-Hill, New York, 1986), Chap. 17, p. 13.
[30]G. Reiss, J. Vancea, and H. Hoffman, Phys. Rev. Lett. **56**, 2100 (1986).
[31]D. A. Neumann, P. F. Micelli, and H. Zabel, Appl. Phys. Lett. **48**, 24 (1986).
[32]B. M. Clemens and J. G. Gay, Phys. Rev. B **35**, 9337 (1987).
[33]*American Institute of Physics Handbook* (McGraw-Hill, New York, 1972). The thermal diffusivity is calculated from values of the heat capacity and thermal conductivity interpolated to room temperature.
[34]C. Kittel, *Introduction to Solid State Physics* (Wiley, New York, 1971). The electron mean free path (l) can be estimated from the relation $K=\frac{1}{3}C_e v_f l$, where C_e is the electronic specific heat and v_f is the Fermi velocity. Using C_e values and K values for bulk Ti and Zr (Ref. 33) and assuming $v_f \approx 10^6$ m/sec, we obtain $l \approx 2$ nm. Further degradation of l will result from structural disorder, as evidenced by our measured values of thermal diffusivity which are an order of magnitude lower than bulk values.
[35]G. L. Eesley, B. M. Clemens, and C. A. Paddock, Appl. Phys. Lett. **50**, 717 (1987).
[36]J. A. Nelder and R. Mead, Comput. J. **7**, 308 (1965).

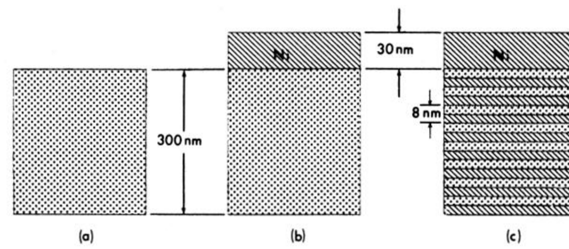

FIG. 1. Sample geometry: (a) single-element film; (b) bilayer film; (c) multilayer film. Both the bilayer and multilayer films are capped with 30 nm of Ni.